

Dynamic properties of the magnetic skyrmion driven by electromagnetic waves with spin angular momentum and orbital angular momentum

Longfei Guo(郭龙飞), Bing Zha(查兵), Xiaoqiao Sun(孙晓乔), Songmei Ni(倪松梅), Ruiyu Huang(黄瑞玉), Lin Chen(陈琳), and Zhikuo Tao(陶志阔)

Citation: Chin. Phys. B, 2024, 33 (**11**): 117501. DOI: 10.1088/1674-1056/ad7577
Journal homepage: http://cpb.iphy.ac.cn; http://iopscience.iop.org/cpb

What follows is a list of articles you may be interested in

Dzyaloshinskii-Moriya interaction and field-free sub-10 nm topological magnetism in Fe/bismuth oxychalcogenides heterostructures

Yaoyuan Wang(王垚元), Long You(游龙), Kai Chang(常凯), and Hongxin Yang(杨洪新)
Chin. Phys. B, 2024, 33 (**9**): 097508. DOI: 10.1088/1674-1056/ad6a0e

Frequency combs based on magnon-skyrmion interaction in magnetic nanotubes

Tijjani Abdulrazak, Xuejuan Liu(刘雪娟), Zhejunyu Jin(金哲珺雨), Yunshan Cao(曹云姗), and Peng Yan(严鹏)
Chin. Phys. B, 2024, 33 (**8**): 087503. DOI: 10.1088/1674-1056/ad4ff5

Shape-influenced non-reciprocal transport of magnetic skyrmions in nanoscale channel

Jie-Yao Chen(陈杰尧), Jia Luo(罗佳), Geng-Xin Hu(胡更新), Jun-Lin Wang(王君林), Guan-Qi Li(李冠祺), Zhen-Dong Chen(陈振东), Xian-Yang Lu(陆显扬), Guo-Ping Zhao(赵国平), Yuan Liu(刘远), Jing Wu(吴竞), and Yong-Bing Xu(徐永兵)
Chin. Phys. B, 2024, 33 (**7**): 077505. DOI: 10.1088/1674-1056/ad34c7

Creation and annihilation of artificial magnetic skyrmions with the electric field

Jun Cheng(程军), Liang Sun(孙亮), Yike Zhang(张一可), Tongzhou Ji(吉同舟), Rongxing Cao(曹荣幸), Bingfeng Miao(缪冰锋), Yonggang Zhao(赵永刚), and Haifeng Ding(丁海峰)
Chin. Phys. B, 2024, 33 (**3**): 037501. DOI: 10.1088/1674-1056/ad188f

Oscillation of Dzyaloshinskii-Moriya interaction driven by weak electric fields

Runze Chen(陈润泽), Anni Cao(曹安妮), Xinran Wang(王馨苒), Yang Liu(柳洋), Hongxin Yang(杨洪新), and Weisheng Zhao(赵巍胜)
Chin. Phys. B, 2024, 33 (**2**): 027501. DOI: 10.1088/1674-1056/ad0f85

Dynamic properties of the magnetic skyrmion driven by electromagnetic waves with spin angular momentum and orbital angular momentum

Longfei Guo(郭龙飞), Bing Zha(查兵), Xiaoqiao Sun(孙晓乔), Songmei Ni(倪松梅), Ruiyu Huang(黄瑞玉), Lin Chen(陈琳), and Zhikuo Tao(陶志阔)†

College of Electronic and Optical Engineering & College of Flexible Electronics, Nanjing University of Posts and Telecommunications, Nanjing 210003, *China*

(Received 4 June 2024; revised manuscript received 5 August 2024; accepted manuscript online 30 August 2024)

We theoretically studied the dynamic properties of the skyrmion driven by electromagnetic (EM) waves with spin angular momentum (SAM) and orbital angular momentum (OAM) using micromagnetic simulations. First, the guiding centers of the skyrmion driven by EM waves with SAM, i.e., left-handed and right-handed circularly polarized EM waves, present circular trajectories, while present elliptical trajectories under linear EM waves driving due to the superposition of oppositely polarized wave components. Second, the trajectories of the skyrmion driven by EM waves with OAM demonstrate similar behavior to that driven by linearly polarized EM waves. Because the wave vector intensity varies with the phase for both linearly polarized EM waves and EM waves with OAM, the angular momentum is transferred to the skyrmion non-uniformly, while the angular momentum is transferred to the skyrmion uniformly for left-handed and right-handed circularly polarized EM driving. Third, the dynamic properties of the skyrmion driven by EM waves with both SAM and OAM are investigated. It is found that the dynamic trajectories exhibit more complex behavior due to the contributions or competition of SAM and OAM. We investigate the characteristics of intrinsic gyration modes and frequency-dependent trajectories. Our research may provide insight into the dynamic properties of skyrmion manipulated by EM waves with SAM or OAM and provide a method for controlling skyrmion in spintronic devices.

Keywords: skyrmion, spin angular momentum, orbital angular momentum, dynamic properties

PACS: 75.30.Ds, 75.80.+q, 85.70.Ay, 12.39.Dc **DOI:** 10.1088/1674-1056/ad7577

1. Introduction

As a vortex-like topological magnetic soliton with quasi-particle characteristics,[1–3] skyrmion exhibits peculiar physical properties, such as small size and topological stability, which can be used in the design of non-volatile spintronics devices with high density and low energy consumption.[4–6] Using neutron scattering experiments, Mühlbauer *et al.* discovered a two-dimensional lattice of magnetic skyrmion lines in the chiral magnet MnSi, indicating the existence of magnetic skyrmions.[7] In these chiral materials, the competition between DMI and the exchange interaction, Zeeman energy and magnetocrystalline anisotropies cooperatively determine the magnetic topological structures.[8–16]

In recent years, the dynamical properties of skyrmion have received much attention due to their important applications in high-performance, non-volatile spintronic devices.[17–22] The mastery of skyrmion dynamics helps us to achieve precise control of skyrmion motion modes, which include breathing mode[23–25] and gyometric mode[22,26–28] in spintronic devices. It has been shown that the breathing mode of skyrmion is mainly caused by a perpendicularly oscillating magnetic field along the z-axis, while the gyometric mode of skyrmion including clockwise (CW) gyration mode and counter-clockwise (CCW) gyration mode can be excited by an in-plane microwave magnetic field.[22,28] Creating skyrmions,[29] manipulating their shapes[30] and even breaking the topological protection of skyrmions by the excitation of spin-wave modes can be achieved by applying a microwave magnetic field.[31]

In addition, electromagnetic (EM) waves with momentum can also manipulate the dynamic properties of skyrmion, which will provide a new way to design the skyrmion-based devices.[32,33] The typical angular momentum of EM waves includes spin angular momentum (SAM) and orbital angular momentum (OAM).[34] Due to the novel physical characteristics, EM waves with angular momentum have attracted attention in applications from optical data storage to quantum communications. By transferring the angular momentum to the topological magnetic quasi-particles, such as skyrmion, effective manipulation of the dynamic motion can be realized.[33,35] In this paper, we investigate the dynamic properties of the magnetic skyrmion driven by EM waves with SAM and OAM. The simulation methods are presented in Section 2. Subsections 3.1 and 3.2 present the simulation results and discussion on the dynamic properties of the skyrmion driven by EM waves with SAM and OAM, respectively. Then, Subsection 3.3 presents the dynamic properties of the skyrmion driven by EM waves with both SAM and OAM. Finally, the conclusion is presented in Section 4.

†Corresponding author. E-mail: zktao@njupt.edu.cn

© 2024 Chinese Physical Society and IOP Publishing Ltd

2. Simulation methods

The dynamic properties of skyrmion driven by electromagnetic microwave with SAM and OAM are simulated using Object-Oriented MicroMagnetic Framework (OOMMF) open-source software.[36] In order to obtain the static states and dynamic response of skyrmion, numerical solutions of the Landau–Lifshitz–Gilbert (LLG) equation are performed.[37] The LLG equation can be described as

$$\frac{\partial \boldsymbol{m}(r,t)}{\partial t} = -\mu_0\gamma(\boldsymbol{m}(r,t)\times\boldsymbol{H}_{\text{eff}}) + \alpha[\boldsymbol{m}(r,t)\times\frac{\partial \boldsymbol{m}(r,t)}{\partial t}], \quad (1)$$

where α is the phenomenological Gilbert damping parameter, γ is the gyromagnetic ratio, μ_0 is the vacuum permeability and $\boldsymbol{m}(r,t)$ is the normalized magnetization. $\boldsymbol{H}_{\text{eff}}$ is the effective magnetic field, which can be computed by

$$\boldsymbol{H}_{\text{eff}} = -\frac{1}{\mu_0 M_{\text{s}}}\frac{\partial E_{\text{tot}}}{\partial \boldsymbol{m}(r,t)}, \quad (2)$$

where M_{s} denotes the saturation magnetization and E_{tot} is the total energy of the magnetic system. The E_{tot} can be given by

$$E_{\text{tot}} = E_{\text{ex}} + E_{\text{K}} + E_{\text{d}} + E_{\text{Zeeman}} + E_{\text{DM}}. \quad (3)$$

The static state can be determined by comparing the effects of various energy terms, including E_{ex} for exchange energy, E_{K} for anisotropy energy, E_{d} for demagnetization energy, E_{Zeeman} for Zeeman energy and E_{DM} for Dzyaloshinskii–Moriya (DM) interaction energy. Through numerical calculations to minimize the total free energy, denoted as E_{tot}, we can ascertain the ground static state. In this study, the dynamic properties of skyrmion driven by light with spin and orbit angular momentum are investigated, and it is found that the most critical energy component is Zeeman energy, which represents the influence of the external field. Zeeman energy is defined by

$$E_{\text{Zeeman}} = -\mu_0 M_{\text{s}}\int \boldsymbol{m}(r,t)\cdot\boldsymbol{H}_{\text{ext}}\,\text{d}V. \quad (4)$$

In the given equation, μ_0 represents the magnetic permeability in vacuum, $\boldsymbol{m}(r,t)$ stands for the magnetization vector within the system and $\boldsymbol{H}_{\text{ext}}$ denotes the applied external field, which is related to the characteristics of light with SAM and OAM. Furthermore, both circularly polarized EM waves with SAM can be achieved by superposing two linearly polarized EMs along the x- and y-directions with a phase difference of $\pm\pi/2$ (supposing the wave is traveling along the z-direction). Furthermore, EM waves with OAM can be achieved by superposing an oscillating magnetic field with a spiral phase factor.

In this study, we focused on the dynamic properties of Bloch-type skyrmions. Bloch-type skyrmions were formed in an FeGe disk with a radius of 50 nm and a thickness of 5 nm. In the simulations, the typical parameters in the FeGe system are as follows: exchange stiffness constant $A = 0.4\times10^{-11}$ J/m, saturation magnetization constant $M_{\text{s}} = 3.84\times10^5$ A/m. The external applied static magnetic field H_0 is set at 1×10^5 A/m and DMI constant D is set at 0.718×10^{-3} J/m^2. In all simulations, a mesh size of $5\times5\times5$ nm^3 is used. The gyromagnetic ratio γ_0 is fixed at 2.211×10^5 m·A^{-1}·s^{-1} and damping coefficient α is fixed at 0.05. For microwave with SAM, the amplitude of the dynamic magnetic field H_1 is set at 1×10^3 A/m. For microwave with OAM, the width of the beam waist w is configured at 40 nm and the magnetic field strength is 1×10^3 A/m.

3. Results and discussion

3.1. Dynamic properties of skyrmion driven by EM waves with SAM

First, we investigate the dynamic properties of a skyrmion driven by an EM wave with SAM. As depicted in Fig. 1(a), the propagation direction of the EM waves is perpendicular to the plane of the skyrmion. In order to illustrate the dynamic trajectories of the skyrmion driven by EM waves, the guiding centers (R_x, R_y) of the skyrmion are calculated as[38–41]

$$R_x = \frac{\iint xq\,\text{d}x\text{d}y}{\iint q\,\text{d}x\text{d}y}, \quad R_y = \frac{\iint xq\,\text{d}x\text{d}y}{\iint q\,\text{d}x\text{d}y}, \quad (5)$$

where q represents the topological density, which can be described as

$$q = \boldsymbol{m}\cdot\left(\frac{\partial \boldsymbol{m}}{\partial x}\times\frac{\partial \boldsymbol{m}}{\partial y}\right). \quad (6)$$

Figures 1(b) and 1(c) are the guiding center trajectories of a skyrmion driven by left-handed circularly polarized and right-handed circularly polarized EM waves with changing frequencies from 10 GHz to 50 GHz, respectively. Figure 1(d) is the relation of the trajectory diameter and driving frequency for left-handed (blue line) and right-handed (red line) circularly polarized EM waves.

It can be seen from Figs. 1(b) and 1(c) that the guiding center trajectories of the skyrmion driven by the EM waves with SAM are circular, and the directions of the trajectories are consistent with the rotation directions of the driving circularly polarized EM waves. Moreover, the trajectory radius varies with the driving frequency. To further investigate the relationship between the trajectory radius and the driving frequency, we present the dependencies of the trajectory diameter on the driving frequency for left-handed (blue line) and right-handed (red line) circularly polarized EM waves, as illustrated in Fig. 1(d). It is evident that the trajectory diameters exhibit an initial increase followed by a decrease within the frequency range of 0–50 GHz for both left-handed and right-handed circularly polarized EM waves. The trajectory diameter reaches its maximum value for left-handed polarized EM waves at a frequency of approximately 1.75 GHz, whereas the maximum diameter occurs at around 13.85 GHz for right-handed polarized EM waves. It has been reported that the gyration motions with opposite rotation direction corresponding to left-handed (CCW) or right-handed (CW) modes can be obtained by solving Thiele's equation by considering gyro-tropic, conservative and viscous forces.[28,40,42,43]

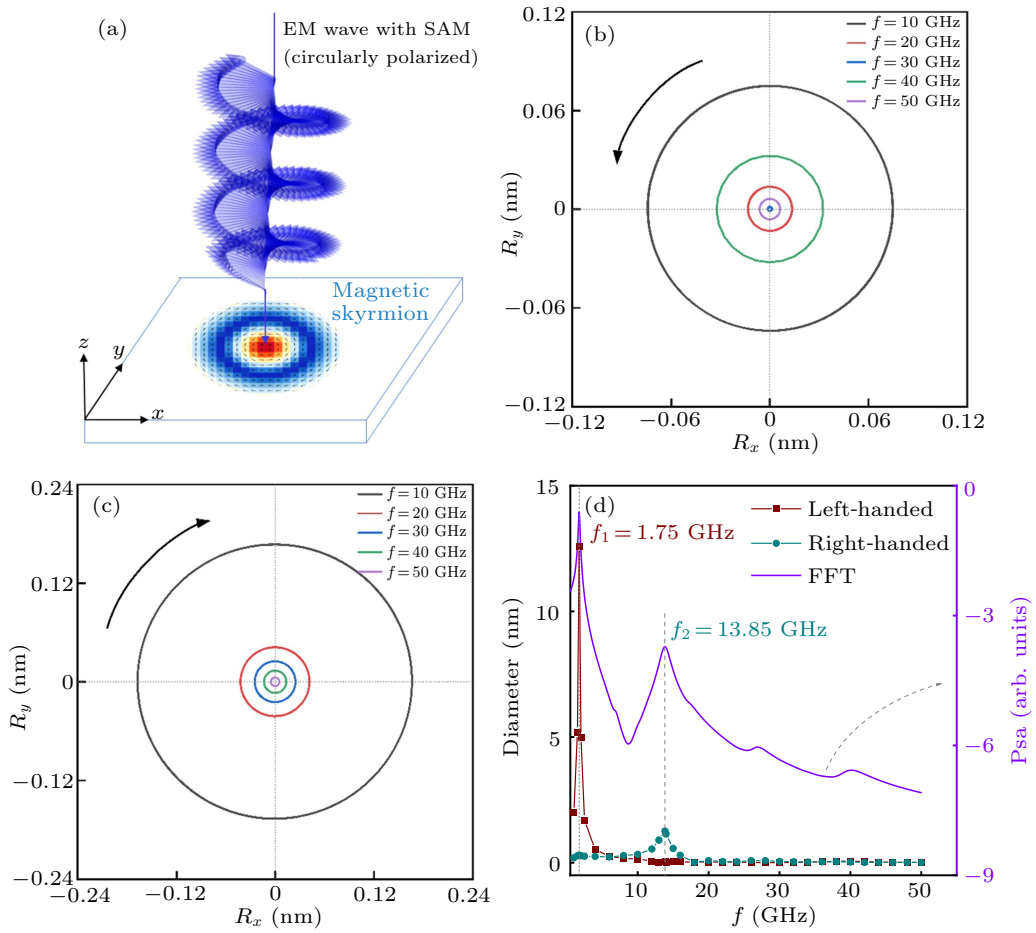


Fig. 1. (a) Skyrmion driven by an EM wave with SAM. Guiding center trajectories of skyrmion driven by (b) left-handed circularly polarized and (c) right-handed circularly polarized EM waves with changing frequencies from 10 GHz to 50 GHz. (d) Relation of trajectory diameter and driving frequency for left-handed (blue line) and right-handed (red line) circularly polarized EM waves, and FFT spectra (purple line) corresponding to magnetization evolution inplused by sinc-function magnetic field.

To elucidate the dynamic characteristics driven by EM waves with SAM, we conducted a detailed investigation into the dynamic behavior of the skyrmion driven by linearly polarized EM waves. Here, dynamic properties of skyrmion driven by linearly polarized EM waves with sinc-function magnetic field are investigated. The sinc-function magnetic field was driven for 20 ns and evolution of the average magnetization over the entire region was recorded. Then, the power spectra from the fast Fourier transform (FFT) denoted by the purple line in Fig. 1(d) was obtained. Two eigenfrequencies (f_1 and f_2) of the skyrmion are observed here and they correspond to the frequencies at which the maximum diameters are achieved driven by left or right-handed circularly polarized EM waves.

Furthermore, dynamic properties of the skyrmion driven by linearly polarized EM waves with a sin-function magnetic field are investigated with frequency changing from 1 GHz to 15 GHz. The guiding centers perform elliptical trajectories with varied major and minor axes for different frequencies. In particular, the trajectories also perform left-handed (CCW) or right-handed (CW) with different frequencies. The trajectories of the guiding center driven by linearly polarized EM waves with changing frequency from 4 GHz to 6.51 GHz and from 6.51 GHz to 11.8 GHz are presented in Figs. 2(a) and 2(b). The trajectories perform CCW with $f < 6.51$ GHz and CW with $f < 6.51$ GHz and shrink to an almost linear vibration with $f = 6.51$ GHz. In addition, the trajectories start to become circular when the frequency of the linearly polarized EM waves is set to the eigenfrequency (f_1 or f_2), as shown in the inset of Figs. 2(a) and 2(b).

The relations of elliptical trajectory characteristics and driving frequency for linearly polarized EM waves are shown in Fig. 2(c). The major axis $2a$, minor axis $2b$ and θ represent the major axis of the steady elliptical trajectory of the skyrmion, the minor axis of the steady elliptical trajectory of the skyrmion and the angular position between the major axis and the $-x$ axis, respectively. As shown in Fig. 2(c), both $2a$ and $2b$ form obvious peaks at 1.75 GHz and weak peaks at 13.85 GHz, which are eigenfrequencies (f_1 and f_2). At the same time, the angular θ keeps increasing from $-30.8°$ to $220.9°$ with driving frequency changing from 1 GHz to 15 GHz.

It is noted that the trajectory of the skyrmion guiding center driven by the linearly polarized EM waves can be considered to be a superposition of the trajectories driven by left-

handed and right-handed circularly polarized EM waves. This is due to the fact that the linearly polarized EM waves can be generated by the superposition of left-handed and right-handed circularly polarized EM waves, which will lead to CCW mode and CW mode, respectively. Figure 3 illustrates the trajectories of the guiding center driven by left-handed circularly polarized, right-handed circularly polarized and linearly polarized EM waves at frequencies of 1.75 GHz, 4 GHz, 6.51 GHz, 10 GHz, and 13.85 GHz.

Meanwhile, it is found that major axis $2a$ and the minor axis $2b$ of the trajectory driven by the line-polarized EM waves and diameters D_{left} and D_{right} of the trajectory driven by left-handed and right-handed polarized EM waves satisfy the following relationship: $2a = (D_{\text{left}} + D_{\text{right}})/2$, $2b = |D_{\text{left}} - D_{\text{right}}|/2$. In particular, the diameters D_{left} and D_{right} at $f = 6.51$ GHz are identical, which leads to $2a = (D_{\text{left}} + D_{\text{right}})/2 = D_{\text{left}} = D_{\text{right}}$, $2b = |D_{\text{left}} - D_{\text{right}}|/2 = 0$ and then linearly trajectory is observed. This also explains why trajectory driven by linearly polarized EM waves at $f_1 = 1.75$ GHz is similar to that driven by left-handed circularly polarized EM waves, and why trajectory driven by linearly polarized EM waves at 13.85 GHz is similar to that driven by right-handed circularly polarized EM waves.

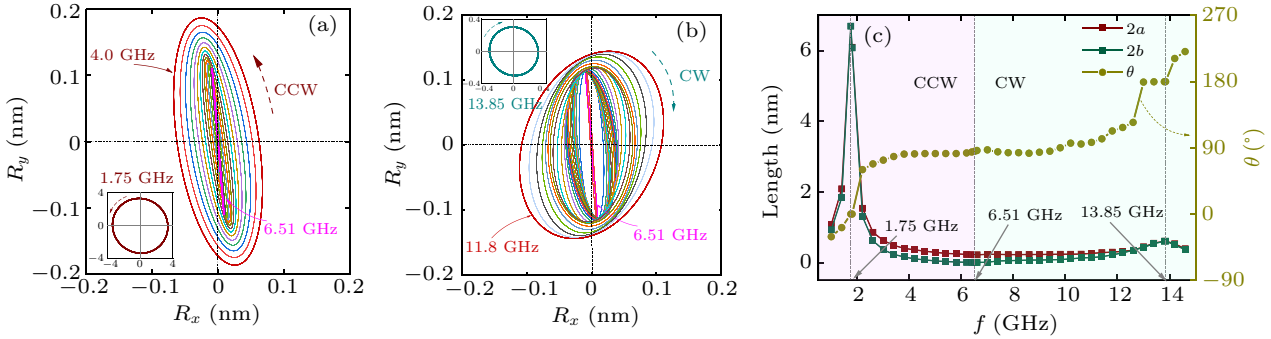


Fig. 2. The trajectories of the guiding center driven by linearly polarized EM waves with changing frequency from 4 GHz to 6.51 GHz (a) and from 6.51 GHz to 11.8 GHz (b). (c) The major axis, minor axis and θ of the elliptical trajectory as a function of the frequency from 1 GHz to 15 GHz.

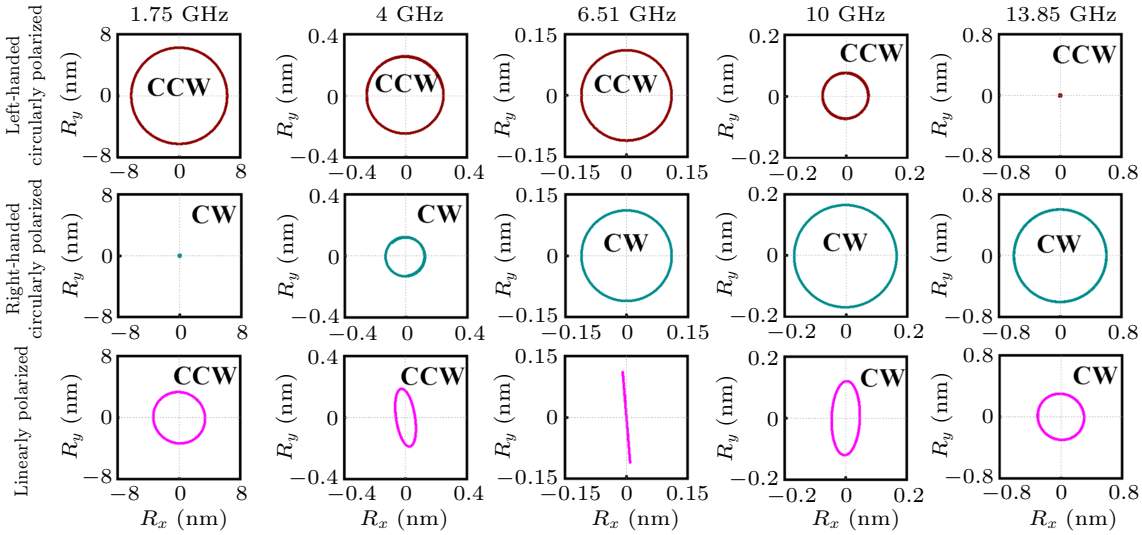


Fig. 3. The trajectories of the guiding center driven by left-handed circularly polarized, right-handed circularly polarized and linearly polarized EM waves at different frequencies of 1.75 GHz, 4 GHz, 6.51 GHz, 10 GHz and 13.85 GHz.

3.2. Dynamic properties of the skyrmion driven by EM waves with OAM

Next, we investigate the dynamic properties of the skyrmion driven by an EM wave with OAM, as shown in Fig. 4(a). The EM waves with OAM exhibit spiral-shaped equiphase surfaces, which can be characterized by a complex amplitude featuring the spiral phase factor $e^{il\phi}$, where l represents the OAM number and ϕ denotes the azimuthal angle. Here, Laguerre–Gaussian EM waves are applied to drive the skyrmion, and the magnetic field of the EM waves can be described as

$$\boldsymbol{H}_{n,l}(\rho,\varphi,t) = H_0' \frac{\left(\frac{\rho}{w}\right)^{|l|} e^{-\frac{\rho^2}{w^2}} L_n^{|l|}\left(2\frac{\rho^2}{w^2}\right)}{\sqrt{w}} e^{i(\omega t - l\varphi)} \boldsymbol{e}_{\text{p}}, \quad (7)$$

where ρ is the radial coordinate, w represents the waist width, H_0' represents the field coefficient and $L_n^{|l|}$ represents the generalized Laguerre function with n denoting the radial index. Yang *et al.* and Guan *et al.* have demonstrated that EM waves with OAM can manipulate the skyrmion motion in ferromagnets[33] and antiferromagnets,[35] respectively. Dif-

ferent from their work, the skyrmion is initially located at the center of the vortex beam during micromagnetic simulation.

Figure 4(b) presents the trajectories of the skyrmion guiding center driven by EM waves with OAM (radial index $n = 1$ and OAM number $l = 2$) with changing frequencies from 10 GHz to 50 GHz. Figures 4(c) and 4(d) are the major axis and the minor axis of the elliptical trajectory with different l from 2 to 10 (where l are all set to even) at different frequencies from 10 GHz to 50 GHz. It can be seen from Fig. 4(b) that the trajectories of the skyrmion driven by EM waves with OAM ($l = 2$) are elliptical and exhibit different shapes under changing frequencies. Moreover, the trajectories present similar performance when the OAM number l is even, such as 4, 6 and 8, which can be seen in Fig. s1. However, the trajectories have an extremely small range of motion confined to about 10^{-14} nm for 50 ns, which indicates that the skyrmion has not been moved when the OAM number l is odd, as depicted in Fig. s2. It is known that the phase of the EM waves with OAM changes continuously from 0 to $2\pi l$ in the angular direction and possesses n+1 cyclic phase periods. In addition, the phase change completes two full periods (inner and outer loop) with a relatively symmetrical phase distribution when l is even, whereas an odd l results in an asymmetric phase change over a complete cycle. Therefore, the angular momentum could not be transferred to the skyrmion and the skyrmion did not move when we put the skyrmion at the center of the beam. In fact, analytical analysis is necessary to explain this effect, and we will continue working on this in a future investigation. Furthermore, the major and minor axes of the trajectory gradually decrease initially, then increase and finally decrease with the increase of l when the frequency ranges from 10 GHz to 50 GHz.

Furthermore, we studied relations of trajectories and driving frequencies under EM waves with OAM ($l = 2$, 4, 6 and 8), as shown in Fig. 5. An obvious peak value of $2a$ can be observed at $f = 2$ GHz with $l = 2$. The inset figure in Fig. 5(a) presents the trajectory of the skyrmion with driving $f = 2$ GHz. Moreover, two peak values of $2a$ can be observed with $l = 4$, 6 and 8. The inset figures in Figs. 5(b)–5(d) present the trajectories of the skyrmion with the peak driving frequencies. The first trajectory with $l = 2$, 4, 6 and 8 presents as elliptical, while the second trajectory with $l = 4$, 6 and 8 presents as almost circular. In particular, the first trajectory or second trajectory alternates between CCW and CW with increasing l and the two trajectories show different directions of rotation. In addition, we calculated the relations of elliptical θ and driving frequencies under EM waves with OAM ($l = 2$, 4, 6 and 8), as shown in Fig. s3 in the supplementary material and we did not find obvious regular characteristics. We find the existence of linear vibration when $l = 4$ of EM waves with OAM, as shown in Fig. s4, which is the same as the dynamic properties of a skyrmion driven by linear EM waves, where the conversion between these two elliptical modes is achieved by a transition to linear vibration.

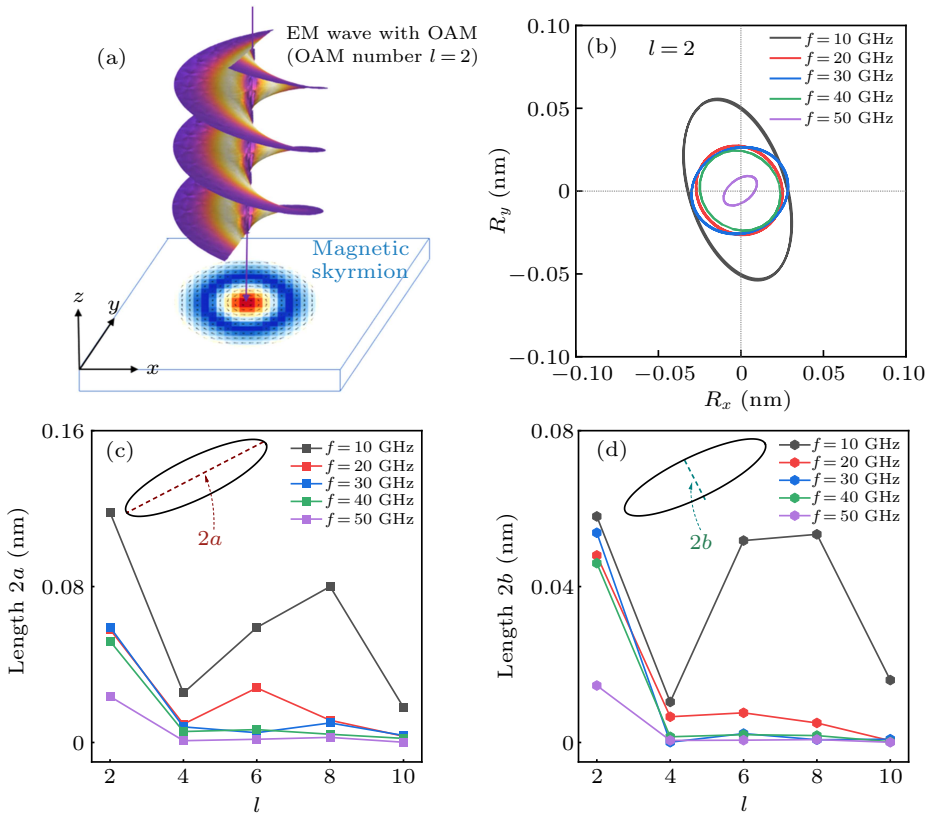


Fig. 4. (a) Skyrmion driven by an EM wave with OAM. (b) Guiding center trajectories of skyrmion driven by EM waves with OAM (radial index $n = 1$ and OAM number $l = 2$) with changing frequencies from 10 GHz to 50 GHz. (c) The major axis and (d) minor axis of the elliptical trajectory with different l from 2 to 10 at different frequencies from 10 GHz to 50 GHz.

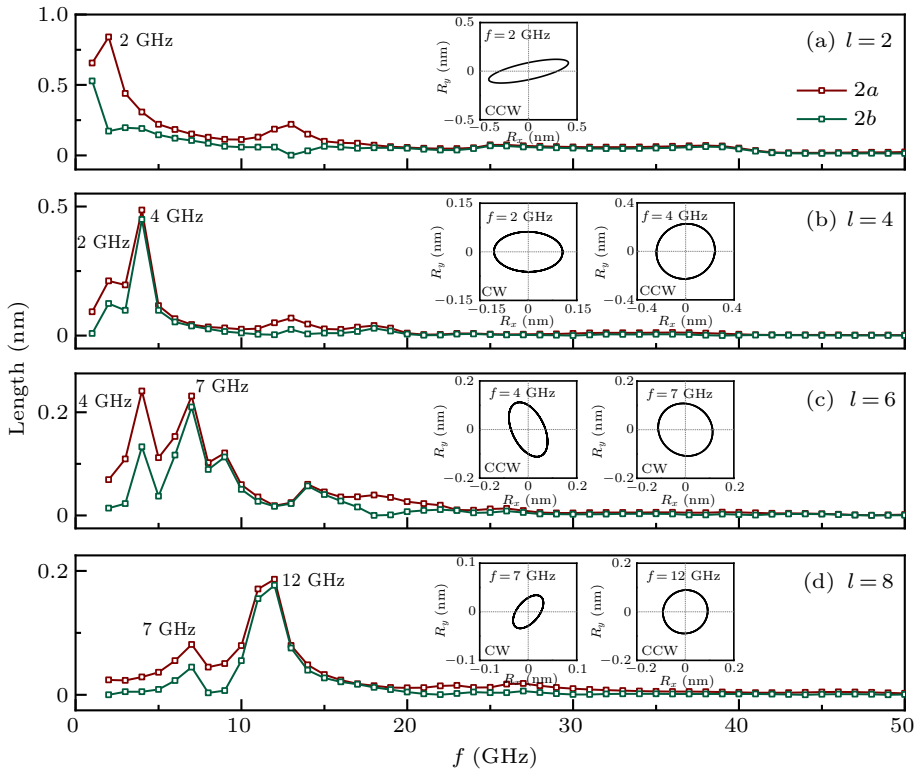


Fig. 5. Relations of trajectories and driving frequencies under EM waves with OAM. (a) $l = 2$, (b) $l = 4$, (c) $l = 6$ and (d) $l = 8$.

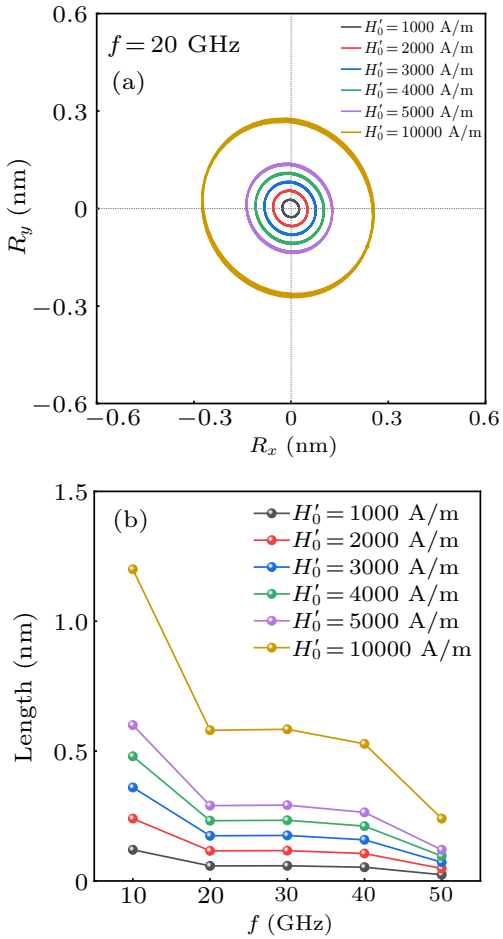


Fig. 6. (a) Guiding center trajectories of skyrmion driven by EM waves with OAM ($l = 2$, $f = 20$ GHz) with changing H_0' from 1000 A/m to 10000 A/m. (b) The major axis of the elliptical trajectory as a function of the frequency from 10 GHz to 50 GHz under different H_0'.

In addition, the dynamics of skyrmion driven by EM waves with changing magnetic field coefficient H_0' (presented in Eq. (7)) has been investigated, as shown in Figs. 6(a) and 6(b). This field coefficient H_0' represents the strength of the EM waves with OAM. At the same time, the dynamics of skyrmion under different static magnetic field H_0 has also been investigated, as shown in Figs. s6(a) and s6(b) in the supplementary material. The static field H_0 can manipulate the topological structure of the skyrmion.

Figure 6(a) presents the guiding center trajectories of skyrmion driven by EM waves with OAM ($l = 2$, $f = 20$ GHz) with changing H_0' from 1000 A/m to 10000 A/m. It can be seen that the R_x and R_y are increased with increasing the strength of H_0'. The major axis of the elliptical trajectory as a function of the frequency from 10 GHz to 50 GHz under different H_0' are shown in Fig. 6(b). It can be seen that the major axis drops obviously with the frequency increasing from 10 GHz to 20 GHz or from 40 GHz to 50 GHz under each H_0' and remains stable with the frequency increasing from 20 GHz to 40 GHz. In particular, the value of the major axis is proportional to the strength of H_0' for each driving frequency. A similar trend with different H_0 is observed in Fig. s6(b) in the supplementary material.

3.3. Dynamic properties of skyrmion driven by EM waves with SAM and OAM

Finally, the dynamic properties of skyrmion driven by EM waves with both SAM and OAM are investigated. Here, the left-handed EM waves presented in Figs. 7(a) and7(b) and

right-handed EM waves presented in Figs. 7(c)–7(e) carry the SAM, while the EM waves with OAM hold $l = 2$. It can be seen that the guiding center trajectories keep CCW under driving frequency ranging from 10 GHz to 50 GHz with SAM (left-handed) and OAM ($l = 2$), as shown in Fig. 7(a), while the trajectories keep CW under driving frequency of 10 GHz and 20 GHz, but change to the present CCW under driving frequency of 30 GHz, 40 GHz and 50 GHz with SAM (right-handed) and OAM ($l = 2$), as shown in Figs. 7(d) and 7(e).

We have presented that the guiding center trajectories hold CCW under left-handed EM wave driving or CW under right-handed EM wave driving at each simulated frequency. However, the guiding center trajectories present CCW or CW under EM waves with OAM driving at different frequencies. Considering that R_x and R_y can be also manipulated with the magnetic field strength, the driving frequency, the OAM number and other key parameters, the trajectories will exhibit complex behavior due to the competition between SAM and OAM.

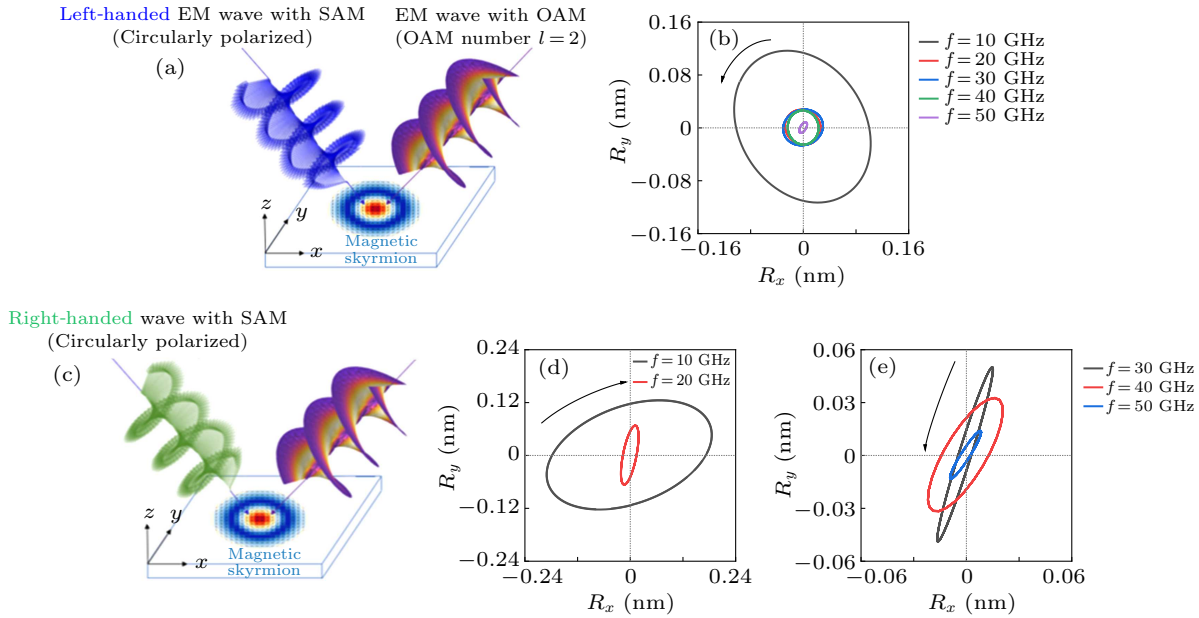


Fig. 7. Skyrmion driven by an EM wave with (a) OAM and SAM (left-handed circularly polarized), (c) OAM and SAM (right-handed circularly polarized), (b) guiding center trajectories of skyrmion driven by an EM wave with OAM and SAM (left-handed). Guiding center trajectories of skyrmion driven by an EM wave with OAM and SAM (right-handed) with (d) $f = 10$ GHz and 20 GHz, (e) $f = 30$ GHz–50 GHz.

4. Conclusion

In summary, we investigate dynamic properties of the skyrmion driven by EM waves with SAM and OAM. First, we demonstrate the dynamic trajectories of the skyrmion driven by EM waves with SAM (left-handed and right-handed circularly polarized). It is found that the skyrmions present circular trajectories with SAM, and present elliptical trajectories under linear EM waves driving due to the superposition of left-handed and right-handed circularly polarized wave components. Next, the dynamic properties of the skyrmion driven by EM waves with OAM are investigated. We find that the dynamic properties are similar to the dynamic properties driven by linearly polarized EM waves. It is suggested that the wave vector intensity varies with the phase for linearly polarized EM waves and EM waves with OAM, which makes the angular momentum non-uniformly transferred to the skyrmion, while the intensity of left-handed and right-handed circularly polarized EM does not change with the phase, which makes the angular momentum uniformly transferred to the skyrmion, resulting in circular trajectories. Moreover, the dynamic properties of skyrmion driven by EM waves with both SAM and OAM are investigated. It is found that the dynamic trajectories exhibit more complex behavior due to the contribution of both SAM and OAM. In addition, there are still some problems with simulating the dynamic properties when the skyrmion is driven by EM waves with negative OAM numbers. This took much more time for simulation than that with positive OAM numbers. This may be due to the different physical interaction mechanisms of skyrmion driven by vortex with negative and positive l, and we are still trying to understand this. However, our simulation results may contribute to the understanding of dynamic characteristics of skyrmion driven by EM waves with angular momentum, and provide a method for designing spintronic EM wave devices based on skyrmion.

References

[1] Skyrme T H R 1962 *Nucl. Phy.* **31** 556
[2] Skyrme T H R 1961 *Proc. R. Soc. London Ser. A* **262** 237
[3] Skyrme T H R 1961 *Proc. R. Soc. London Ser. A* **260** 127
[4] Fert A, Reyren N and Cros V 2017 *Nat. Rev. Mater.* **2** 17031
[5] Göbel B, Mertig I and Tretiakov O A 2021 *Phys. Rep.* **895** 1
[6] Marrows C and Zeissler K 2021 *Appl. Phys. Lett.* **119** 250520
[7] Mühlbauer S, Binz B, Jonietz F, Pfleiderer C, Rosch A, Neubauer A, Georgii R and Böni P 2009 *Science* **323** 915
[8] Moriya T 1960 *Phys. Rev. Lett.* **4** 228

[9] Münzer W, Neubauer A, Adams T, Mühlbauer S, Franz C, Jonietz F, Georgii R, Böni P, Pedersen B and Schmidt M 2010 *Phys. Rev. B* **81** 041203

[10] Shibata K, Yu X, Hara T, Morikawa D, Kanazawa N, Kimoto K, Ishiwata S, Matsui Y and Tokura Y 2013 *Nat. Nanotechnol.* **8** 723

[11] Yu X, Kanazawa N, Onose Y, Kimoto K, Zhang W, Ishiwata S, Matsui Y and Tokura Y 2011 *Nat. Mater.* **10** 106

[12] Woo S, Litzius K, Krüger B, Im M Y, Caretta L, Richter K, Mann M, Krone A, Reeve R M and Weigand M 2016 *Nat. Mater.* **15** 501

[13] Henderson M, Bleuel M, Beare J, Cory D, Heacock B, Huber M, Luke G, Pula M, Sarenac D and Sharma S 2022 *Phys. Rev. B* **106** 094435

[14] Birch M, Moody S, Wilson M, Crisanti M, Bewley O, Štefančič A, Balakrishnan G, Fan R, Steadman P and Venero D A 2020 *Phys. Rev. B* **102** 104424

[15] Bak P and Jensen M H 1980 *J. Phys. C: Solid State Phys.* **13** L881

[16] Nagaosa N and Tokura Y 2013 *Nat. Nanotechnol.* **8** 899

[17] Tomasello R, Martinez E, Zivieri R, Torres L, Carpentieri M and Finocchio G 2014 *Sci. Rep.* **4** 6784

[18] Sampaio J, Cros V, Rohart S, Thiaville A and Fert A 2013 *Nat. Nanotechnol.* **8** 839

[19] Mochizuki M, Yu X, Seki S, Kanazawa N, Koshibae W, Zang J, Mostovoy M, Tokura Y and Nagaosa N 2014 *Nat. Mater.* **13** 241

[20] Kong L and Zang J 2013 *Phys. Rev. Lett.* **111** 067203

[21] Everschor K, Garst M, Binz B, Jonietz F, Mühlbauer S, Pfleiderer C and Rosch A 2012 *Phys. Rev. B* **86** 054432

[22] Moon K W, Kim D K, Je S G, Chun B S, Kim W, Qiu Z, Choe S B and Hwang C 2016 *Sci. Rep.* **6** 20360

[23] Kim J V, Garcia-Sanchez F, Sampaio J, Moreau-Luchaire C, Cros V and Fert A 2014 *Phys. Rev. B* **90** 064410

[24] McKeever B, Rodrigues D, Pinna D, Abanov A, Sinova J and Everschor-Sitte K 2019 *Phys. Rev. B* **99** 054430

[25] Garanin D A, Jaafar R and Chudnovsky E M 2020 *Phys. Rev. B* **101** 014418

[26] Wang W, Beg M, Zhang B, Kuch W and Fangohr H 2015 *Phys. Rev. B* **92** 020403

[27] Jin C D, Song C K, Wang J S, Xia H Y, Wang J B and Liu Q F 2017 *J. Appl. Phys.* **122** 223901

[28] Mochizuki M 2012 *Phys. Rev. Lett.* **108** 017601

[29] Vigo-Cotrina H and Guimarães A 2020 *J. Magn. Magn. Mater.* **507** 166848

[30] Mehmood N, Wang J, Zhang C, Zeng Z, Wang J and Liu Q 2022 *J. Magn. Magn. Mater.* **545** 168775

[31] Shen X, Zhao R, Ji L, Hu C, Ren W, Chen W, Li Y, Zhang J, Zhang X and Dong X 2022 *J. Magn. Magn. Mater.* **541** 168521

[32] Liu Y, Liu T, Jin Z, Hou Z, Chen D, Fan Z, Zeng M, Lu X, Gao X and Qin M 2022 *Phys. Rev. B* **106** 064424

[33] Yang W, Yang H, Cao Y and Yan P 2018 *Opt. Express* **26** 8778

[34] Li H, Rodriguez-Fajardo V, Chen P and Forbes A 2020 *Phys. Rev. A* **102** 063533

[35] Guan S H, Liu Y, Hou Z P, Chen D Y, Fan Z, Zeng M, X. Lu X B, Gao X S, Qin M H and Liu J M 2023 *Phys. Rev. B* **107** 214429

[36] Beg M, Lang M and Fangohr H 2022 *IEEE Trans. Magn.* **58** 7300205

[37] Gilbert T L 2004 *IEEE Trans. Mag.* **40** 3443

[38] Papanicolaou N and Tomaras T N 1991 *Nucl. Phys. B* **360** 425

[39] Dai Y Y, Wang H, Tao P, Yang T, Ren W J and Zhang Z D 2013 *Phys. Rev. B* **88** 054403

[40] Wang W W, Beg M, Zhang B, Kuch W and Fangohr H 2015 *Phys. Rev. B* **92** 020403

[41] Yu D X, Sui C W, Schulz D, Berakdar J and Jia C L 2021 *Phys. Rev. Appl.* **16** 034032

[42] Makhfudz I, Krüger B and Tchernyshyov O 2012 *Phys. Rev. Lett.* **109** 217201

[43] Moon K W, Chun B S, Kim W, Qiu Z Q and Hwang C 2014 *Phys. Rev. B* **89** 064413